Geophys. J. Int. (2002) **148,** 320–328

Finite-difference modelling in two-dimensional anisotropic media using a flux-corrected transport technique

D. H. Yang,[1] E. Liu,[2] Z. J. Zhang[3] and J. Teng[3]

[1] *Department of Mathematics, Tsinghua University, Beijing* 100084, *China. E-mail: dhyang@math.tsinghua.edu.cn*
[2] *British Geological Survey, Murchison House, West Mains Road, Edinburgh* EH9 3LA, *UK. E-mail: E.Liu@bgs.ac.uk*
[3] *Institute of Geology & Geophysics, Chinese Academy of Sciences, Beijing* 100101, *China*

Accepted 2001 August 10. Received 2001 July 30; in original form 2001 January 18.

SUMMARY

The conventional finite-difference (FD) method often suffers from numerical dispersion when too few samples per wavelength are used or when models have large velocity contrast, or artefacts caused by source at grid points. In this paper, we present a fast finite-difference scheme that is based on the application of vectors and matrices in 2-D anisotropic media, and obtain the stability equations. Our method is based on a flux-corrected transport (FCT) technique, originating from hydrodynamics, which can be incorporated in the conventional finite-difference method to eliminate the numerical dispersion and source-generated noises. An n–times decoupled absorbing boundary condition is used in our study. Three-component seismograms in a transversely isotropic medium with a vertical symmetry axis (TIV) are generated for two models using the FCT finite-difference modelling. Compared with the results of the reflectivity method and the conventional FD method without the FCT technique and any absorbing boundary treatments, we conclude that our FCT based FD method can is very accurate and efficient in computing synthetic seismograms in general heterogeneous and anisotropic media.

Key words: anisotropic wave propagation, finite-difference method, flux-corrected transport technique, synthetic seismograms

1 INTRODUCTION

With the requirements of large-scale wavefield simulations and the development of parallel algorithms for modelling wave propagation in general anisotropic and heterogeneous media, the finite-difference scheme is a natural choice. Tsingas *et al.* (1990) presented a modelling algorithm that uses a finite-difference operator. Their algorithm is based on a MacCormack-type splitting scheme for modelling wave propagation in transversely isotropic media. Faria & Stoffa (1994) used a finite-difference algorithm to model a 2-D transversely isotropic medium, which is based on the staggered grid scheme. Igel *et al.* (1995) presented a finite-difference algorithm for modelling general anisotropic media. Their method is based on the convolution algorithm and the Taylor series expansion. The pseudospectral method is attractive as the space operators are exact up to the Nyquist frequency. However, it requires the Fourier transform of the wavefield, which is computationally expensive for 3-D anisotropic simulations. Moreover, taking the Fourier transform means that each point interacts with every other point. In some sense, this is unphysical as the interaction in dynamic elasticity is of a local nature. Therefore, it is necessary to take into account local operators as we design a finite-difference scheme for seismic modelling. On the other hand, it is important to consider local difference operators for fast implementation in parallel computers since the nearest-neighbour communication is extremely fast, and large anisotropic models are feasible because of the intrinsic parallelism of the conservation equations.

Unfortunately, the finite-difference method often suffers from unphysical oscillations, i.e. the so-called numerical dispersion or grid dispersion which is caused by the discretization of the wave equations, near large gradients in wave fields or when the computational grid is too coarse. In addition, the source-generated noises (artefacts due to source location at grid points) can also lower the resolution of modelling results, although these can be effectively removed by spatial filtering with a Gaussian window (Igel *et al.* 1995). To eliminate the undesirable ripples and to raise the resolution of wavefield simulations, Boris & Book (1973) and Book *et al.* (1975) developed a flux-corrected transport (FCT) technique to solve the first-order

system of continuity equations in hydrodynamics. Yang *et al.* (1997) and Fei & Larner (1995) have applied the FCT technique to the second-order acoustic equation. Here, we develop this further by incorporating the FCT technique in the finite-difference method to solve the second-order elastic wave equations in general heterogeneous and anisotropic media.

A variety of absorbing boundary conditions for isotropic media have been given for eliminating the unphysical reflection at the grid boundaries (e.g. Clayton & Engquist 1977; Higdon 1987; Sockacki *et al.* 1987; Randal 1988; Chang & McMechan 1989). Zhang *et al.* (1993, 1999) suggested an absorbing boundary condition based on the wave equations in 2-D transversely isotropic media. However, for the boundary equations, different displacement components for elastic waves are still coupled in the same boundary equation. Some boundary conditions, which have repeatedly absorbing ability and are decoupled, are developed in this paper, which is called an n–times decoupled absorbing boundary condition.

The FCT technique presented in this paper is fast and requires little storage space, and it is based on the application of vectors and matrices for modelling elastic propagation in general anisotropic media. To keep numerical calculation stable and accurate we also derive a stability criterion based on the modulus of matrices. Finally, we show examples of three-component VSP synthetic seismograms and our numerical results illustrate that our FCT based FD technique in the conventional finite-difference method is very accurate and efficient.

2 FINITE-DIFFERENCE SCHEME

The elastic-wave equations in a 2-D anisotropic medium can be written as

$$\rho(x,z)\frac{\partial^2 U}{\partial t^2}=\frac{\partial}{\partial x}\left(A\frac{\partial}{\partial x}+C\frac{\partial}{\partial z}\right)U+\frac{\partial}{\partial z}\left(G\frac{\partial}{\partial x}+Q\frac{\partial}{\partial z}\right)U+\bar{F}, \tag{1}$$

where $\rho(x, z)$ is the density, and

$$A=\begin{bmatrix} c_{11} & c_{16} & c_{15} \\ c_{16} & c_{66} & c_{56} \\ c_{15} & c_{56} & c_{55} \end{bmatrix},\quad C=\begin{bmatrix} c_{15} & c_{14} & c_{13} \\ c_{56} & c_{46} & c_{36} \\ c_{55} & c_{45} & c_{35} \end{bmatrix},$$

$$G=\begin{bmatrix} c_{15} & c_{56} & c_{55} \\ c_{14} & c_{46} & c_{45} \\ c_{13} & c_{36} & c_{35} \end{bmatrix},\quad Q=\begin{bmatrix} c_{55} & c_{45} & c_{35} \\ c_{45} & c_{44} & c_{34} \\ c_{35} & c_{34} & c_{33} \end{bmatrix},$$

$$U=\begin{bmatrix} u_x \\ u_y \\ u_z \end{bmatrix},\quad \bar{F}=\begin{bmatrix} f_x \\ f_y \\ f_z \end{bmatrix},$$

where $c_{ij}(x, z)(c_{ij}=c_{ji})$ are elastic constants; u_x, u_y and u_z is the displacement components in x-, y- and z-directions, respectively; f_x, f_y *and* f_z denotes the components of the source in x-, y- and z-directions, respectively. The fact that matrices **A**, **Q**, and **C**+**G** are symmetric is useful for computing the modulus of the matrices.

Adopting the central difference to approximate eq. (1) without the source term $\bar{F}$, we have

$$\begin{aligned} U_{i,j}^{n+1} =& 2U_{i,j}^{n}-U_{i,j}^{n-1}+\left(\frac{\Delta t}{\Delta x}\right)^2\frac{1}{\rho_{i,j}}[A_{i+1/2,j}(U_{i+1,j}^{n}-U_{i,j}^{n}) \\ & -A_{i-1/2,j}(U_{i,j}^{n}-U_{i-1,j}^{n})] \\ & +\left(\frac{\Delta t}{\Delta z}\right)^2\frac{1}{\rho_{i,j}}[Q_{i,j+1/2}(U_{i,j+1}^{n}-U_{i,j}^{n}) \\ & -Q_{i,j-1/2}(U_{i,j}^{n}-U_{i,j-1}^{n})] \\ & +\frac{(\Delta t)^2}{4\Delta x\Delta z}\frac{1}{\rho_{i,j}}[C_{i+1,j}(U_{i+1,j+1}^{n}-U_{i+1,j-1}^{n}) \\ & -C_{i-1,j}(U_{i-1,j+1}^{n}-U_{i-1,j-1}^{n}) \\ & +G_{i,j+1}(U_{i+1,j+1}^{n}-U_{i-1,j+1}^{n}) \\ & -G_{i,j-1}(U_{i+1,j-1}^{n}-U_{i-1,j-1}^{n})], \end{aligned} \tag{2}$$

where Δx and Δz denote the spatial increments in x- and z-directions, respectively; Δt is the time-step size, $U_{i,j}^{n}=U(i\Delta x, j\Delta z, n\Delta t)$, and

$$A_{i+1/2,j}=\frac{1}{2}(A_{i+1,j}+A_{i,j}),\quad Q_{i,j+1/2}=\frac{1}{2}(Q_{i,j+1}+Q_{i,j}),$$

where $A_{i,j}=A(i\Delta x, j\Delta z)$, $Q_{i,j}=(i\Delta x, j\Delta z)$, and $G_{i,j}=G(i\Delta x, j\Delta z)$.

3 THE STABILITY CRITERION

Richtmyer & Morton (1967) presented a variety of stability analyses. According to their energy method, and through a series of mathematical operations, we obtain the following stability criterion for the FD scheme in eq. (2)

$$\|A\|\left(\frac{\Delta t}{\Delta x}\right)^2+\|Q\|\left(\frac{\Delta x}{\Delta z}\right)^2\le\rho,\ \textit{if}\ \|C+G\|\le 2\sqrt{\|A\|\cdot\|Q\|},$$

$$\max\left[F(\alpha,\beta),\ \|A\|\left(\frac{\Delta t}{\Delta x}\right)^2+\|Q\|\left(\frac{\Delta t}{\Delta z}\right)^2\right]\le\rho,\quad \textit{if}\ \|C+G\|>2\sqrt{\|A\|\cdot\|Q\|},$$

where functions $F(\alpha, \beta)$, α, β are given by

$$F(\alpha,\beta)=\left(\frac{\Delta t}{\Delta x}\right)^2\|A\|\sin^2\alpha+\left(\frac{\Delta t}{\Delta z}\right)^2\|Q\|\sin^2\beta+\frac{(\Delta t)^2}{4\Delta x\Delta z}\|C+G\|\sin 2\alpha\sin 2\beta,$$

$$\sin 2\alpha=\frac{\|Q\|}{\|C+G\|^2}\left[\frac{\|C+G\|^4-16\|A\|^2\cdot\|Q\|^2}{K^4\|A\|^2+\|Q\|^2}\right]^{1/2},$$

$$\sin 2\beta=\frac{K\|C+G\|\sin 2\alpha}{\sqrt{4\|Q\|^2+K^2\|C+G\|^2\sin^2 2\alpha}},$$

where $K=\Delta z/\Delta x$, and $\|\cdot\|$ denotes a matrix modulus.

In isotropic media, through computing the modulus of the matrices **A**, **Q**, and **C**+**G**, for the FD scheme in eq. (2), we can

obtain the following stability criterion

$$\left(\frac{\Delta t}{\Delta x}\right)^2 \cdot (\lambda + 2\mu) + \left(\frac{\Delta t}{\Delta z}\right)^2 \cdot (\lambda + 2\mu) \leq \rho,$$

or

$$v_p \Delta t \sqrt{\frac{1}{\Delta x^2} + \frac{1}{\Delta z^2}} \leq 1,$$

where λ and μ are the Lamé constants, v_p is the P-wave velocity. The stability condition is independent of the S-wave velocity. Note that the stability criterion given above is the same as that of Aboudi (1971).

As an example, for a transversely isotropic medium, choosing the elastic constants $c_{11}=18$, $c_{13}=6.4$, $c_{33}=12$, $c_{55}=5.5$, $c_{66}=4.2$, then $\|\mathbf{A}\|=18$, $\|\mathbf{Q}\|=12$, $\|\mathbf{C}+\mathbf{G}\|=11.9$.

Obviously, the inequality $\|\mathbf{C}+\mathbf{G}\| \leq 2\sqrt{\|\mathbf{A}\| \cdot \|\mathbf{Q}\|}$ is satisfied under this case, so we have

$$\Delta t \leq \sqrt{\rho \Big/ \left(\frac{18}{\Delta x^2} + \frac{12}{\Delta z^2}\right)}.$$

Detailed analysis for heterogeneous media can be found in Yang (1996). Because the matrices **A**, **Q**, and **C**+**G** are symmetric, the modulus of matrices in the stability criterion given above can be given via their eigenvalues

$$\|A\| = \rho(A),\ \|Q\| = \rho(Q),\ \|C+G\| = \rho(C+G),$$

where $\rho(\mathbf{A})$, $\rho(\mathbf{Q})$ and $\rho(\mathbf{C}+\mathbf{G})$ denote the spectral radii of the matrices **A**, **Q**, and **C**+**G**, respectively.

4 ABSORBING BOUNDARY CONDITIONS

In the finite-difference calculations, an artificial reflection arises at the edges of the model domain. To eliminate this spurious reflection, let

$$\left(\frac{\partial}{\partial t} \pm h \frac{\partial}{\partial x_i}\right)^n u_{x_j} = 0, \tag{3}$$

be a n–time decoupled absorbing boundary condition. Where h is a non-negative parameter determined by elastic constants and density, x_j denotes x or z; u_{x_j} is the displacement component in x_j direction, n denotes absorbing times, the '+' sign is for the right or bottom boundary, and the '−' sign is for the left boundary.

In transversely isotropic media, let $h=\sqrt{c_{11}/\rho}$ or $h=\sqrt{c_{44}/\rho}$ in eq. (3), we can obtain the left and right or bottom absorbing boundary conditions for u_x components. Let $h=\sqrt{c_{66}/\rho}$ or $h=\sqrt{c_{44}/\rho}$, we can obtain the left and right or bottom absorbing boundary conditions for u_y components.

If we choose $n=2$, and $u_{x_j}=u$ in eq. (3), discretizing eq. (3) for different boundaries, we have

$$u_{N,j}^{n+1} = \frac{1}{1+h\cdot\Delta t/\Delta x}\left[2u_{N,j}^n - u_{N,j}^{n-1} - u_{N-2,j}^{n+1} + 2u_{N-2,j}^n - u_{N-2,j}^{n-1} + h\cdot\frac{\Delta t}{\Delta x}\cdot(u_{N-2,j}^{n+1} + u_{N,j}^{n-1} - u_{N-2,j}^{n-1}) - 2h^2\left(\frac{\Delta t}{\Delta x}\right)^2\cdot(u_{N,j}^n - 2u_{N-1,j}^n + u_{N-2,j}^n)\right], \tag{4a}$$

$$u_{0,j}^{n+1} = \frac{1}{1+h\cdot\Delta t/\Delta x}\left[2u_{0,j}^n - u_{0,j}^{n-1} - u_{2,j}^{n+1} + 2u_{2,j}^n - u_{2,j}^{n-1} + h\cdot\frac{\Delta t}{\Delta x}\cdot(u_{2,j}^{n+1} - u_{2,j}^{n-1} + u_{0,j}^{n-1}) - 2h^2\left(\frac{\Delta t}{\Delta x}\right)^2\cdot(u_{2,j}^n - 2u_{1,j}^n + u_{0,j}^n)\right], \tag{4b}$$

$$u_{i,M}^{n+1} = \frac{1}{1+h\cdot\Delta t/\Delta z}\left[2u_{i,M}^n - u_{i,M}^{n-1} - u_{i,M-2}^{n+1} + 2u_{i,M-2}^n - u_{i,M-2}^{n-1} + h\cdot\frac{\Delta t}{\Delta z}\cdot(u_{i,M-2}^{n+1} + u_{i,M}^{n-1} - u_{i,M-2}^{n-1}) - 2h^2\left(\frac{\Delta t}{\Delta z}\right)^2\cdot(u_{i,M}^n - 2u_{i,M-1}^n + u_{i,M-2}^n)\right], \tag{4c}$$

where $i=0$, N are the left and right boundaries, respectively; $j=M$ is for the bottom boundary.

The above analysis is similar to the paraxial absorbing boundary conditions presented by Clayton & Engquist (1977) and Higdon (1987), and is valid for anisotropic wave propagation.

5 THE FCT FINITE-DIFFERENCE ALGORITHM

To eliminate the numerical dispersion caused by discretization of the wave equations, we apply the flux-corrected transport technique developed by Boris & Book (1973) and Book *et al.* (1975) to the second-order elastic wave equations. In general, the FCT based FD algorithm is divided into three main steps: finite-difference iterating (Stage 1), diffusion computation (Stage 2), and offsetting diffusion (Stage 3). The details are described in the Appendix. In the finite-difference calculation step, the discrete eq. (2) is used, which is identical to the conventional FD method. The numerical solutions computed in Stage 1 are smoothed in the diffusion stage to suppress the artificial ripples caused by the grid dispersion. Unfortunately, in the smoothing procedure, the true ripples are also suppressed because the smoothing process is applied to every grid node in the computation regions, resulting in a lowering of the precision of modelling. However the amplitude loss of the true ripples will be recovered through the non-linear offsetting treatments including in Stage 3.

6 NUMERICAL EXAMPLES

To test the accuracy of our FTC method, we compare the synthetic seismograms calculated using FCT method and the anisotropic reflectivity method (Booth & Crampin 1983a,b). We use a three-layered model with parameters given in Table 1. Five receivers are placed in well from $z=144$ m (R1) to $z=192$ m (R5) spaced 12 m apart. The source with frequency $f=10$ Hz Ricker wavelets is located at $z=168$ m and the level distance from the source to the receivers is 456 m. The time variation of the source function is $(1-2\pi^2 f^2 t^2)e^{-(\pi f t)^2}$. The 2-times decoupled absorbing boundary condition is used in FCT numerical calculations. The synthetic VSP seismograms, computed by the FCT and reflectivity method are compared in Fig. 1. The spatial step in the FCT computation is 12 m. The

Table 1. Parameters used in Model 1

Layer (No.)	Thickness (m)	c_{11} (GPa)	c_{13} (GPa)	c_{33} (GPa)	c_{44} (GPa)	c_{66} (GPa)	ρ (g cm^{-3})
1	600	30	8.4	25	10	8	2.1
2	240	20	6.4	19	5.5	4	3.5
3	360	30	8.4	25	10	8	2.1

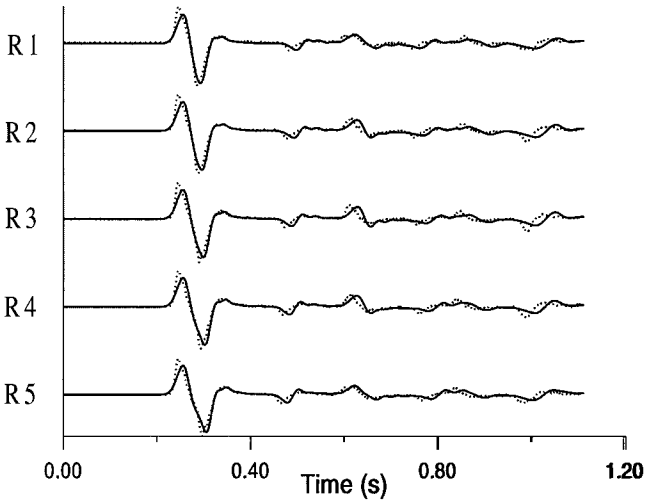

Figure 1. Acoustic seismograms at receivers R1, R2, R3, R4, and R5 in well, generated by the FCTFDM for grid step sizes $\Delta x = \Delta z = 12$ m (solid lines) and anisotropic reflectivity method (dashed lines). The coordinates of the source and receivers R1, R2, R3, R4, and R5 are (504, 168), (960, 144), (960, 156), (960, 168), (960, 180) and (960, 192), respectively.

time steps are 0.6 ms. Fig. 1 shows that the FCTFDM on a coarse grid can provide generally identical result to the reflectivity method.

Synthetic seismograms are generated for two VSP models: one has two layers and the other has four. The parameters are given in Table 2 (Model 2) and Table 3 (Model 3), respectively. Both models are transversely isotropic with a vertical symmetry axis (TIV). In the first model, a grid size of 35 m in x- and z-direction is chosen. The sample rate is 0.002 s. In the second model, a spatial increment of 45 m and a time increment of 0.0025 s are chosen. In both cases, the source is an explosion and has a Ricker wavelet with a peak frequency of 25 Hz. The wavefields are recorded by 119 receivers for Model 2 (139 receivers for Model 3) spread from the surface ($z=0$) to the depth of 4165 m for Model 2 (6255 m for Model 3) spaced 35 m for Model 2 (45 m for Model 3) apart. The source is located at the depth of $z=70$ m and the distance between the source to the first receiver is 3080 m for Model 2 (4860 m for Model 3). Typically a minimum number of 5 grid points per minimum wavelength is required for FD, and this number is reduced to about 2–3 for FCT. On a Pentium III 400 IBM PC with 64 MB RAM, it took about 30 min for Model 2 for and 35 min for Model 3 using standard FD.

Table 2. Parameters used in Model 2

Layer (No.)	Thickness (m)	c_{11} (GPa)	c_{13} (GPa)	c_{33} (GPa)	c_{44} (GPa)	c_{66} (GPa)	ρ (g cm^{-3})
1	2415	30	8.4	25	10	8	2.1
2	1750	20	6.4	19	5.5	4	3.5

Table 3. Parameters used in Model 3

Layer (No.)	Thickness (m)	c_{11} (GPa)	c_{13} (GPa)	c_{33} (GPa)	c_{44} (GPa)	c_{66} (GPa)	ρ (g cm^{-3})
1	2655	40	13	33	12	8	2.0
2	1350	20	6.5	16.5	6	4	2.0
3	675	40	13	33	12	8	2.0
4	1575	20	6.5	16.5	6	4	2.0

Synthetic seismograms generated by the FD method without absorbing boundary conditions are shown in Fig. 2 and the synthetic seismograms computed by the FCT based FD with 2-times decoupled absorbing boundaries are shown in Fig. 3. Fig. 2 is only used as a reference. We can see that the numerical dispersion and boundary reflections are very strong from Fig. 2. In contrast, the seismograms in Fig. 3 are very clean. Furthermore, the *qP*-, *qSV*-, *qSH*-waves, and the reflected, transmitted, and converted waves can all be clearly identified from Fig. 4. Fig. 4 shows the synthetic VSP seismograms computed by the FCT based FD with the 2-times absorbing boundaries for Model 3, we can also identify clearly *qP*-, *qSV*-, *qSH*-waves, and the converted waves although these waveforms are more complicated than these shown in Fig. 3 (Model 2). In addition, different arrival times for *qP*- and *qS*-waves and shear-wave splitting in the anisotropic media can be seen from the synthetic VSP seismograms shown in Figs 3 and 4.

To compare the FCT with the standard FD method, we use the same medium parameters as those of Model 2. The acoustic wave-fields are recorded in a well, and the source is located at $z=816$ m and the level distance from the source to the receivers is 2400 m. The 2-times decoupled absorbing boundary condition is used in numerical calculations. The synthetic VSP seismograms, computed by the FCT and the 4th-order staggered FD code, are shown in Figs 5(a) and (b), respectively. The spatial step in Fig. 5(a) is 24 m, and the spatial step in Fig. 5(b) is 8 m. Figs 5(a,b) show that the FCT can provide same accuracy as the FD method, but need less memory and less computational costs. Actually, the computational speed of the FCT for generating Fig. 5(a) is about 16 times of that of the FD method for generating Fig. 5(b), and the memory of the FCT is about 78 per cent of that of the FD. The computations were performed on a Pentium III 600 with 128 MB memory. It shows that the FCT is more efficient than the standard FD in computer memory and computer speed, and therefore the FCT is more suitable for synthetic VSP seismograms of large models.

7 DISCUSSION AND CONCLUSIONS

It is important to consider local difference operators for parallel computing as the nearest-neighbour communication is extremely fast, and large anisotropic models are feasible because of the intrinsic parallelism of the conservation equations. We have presented a FCT-based FD scheme to model seismic wave propagation in general anisotropic media. This method is fast

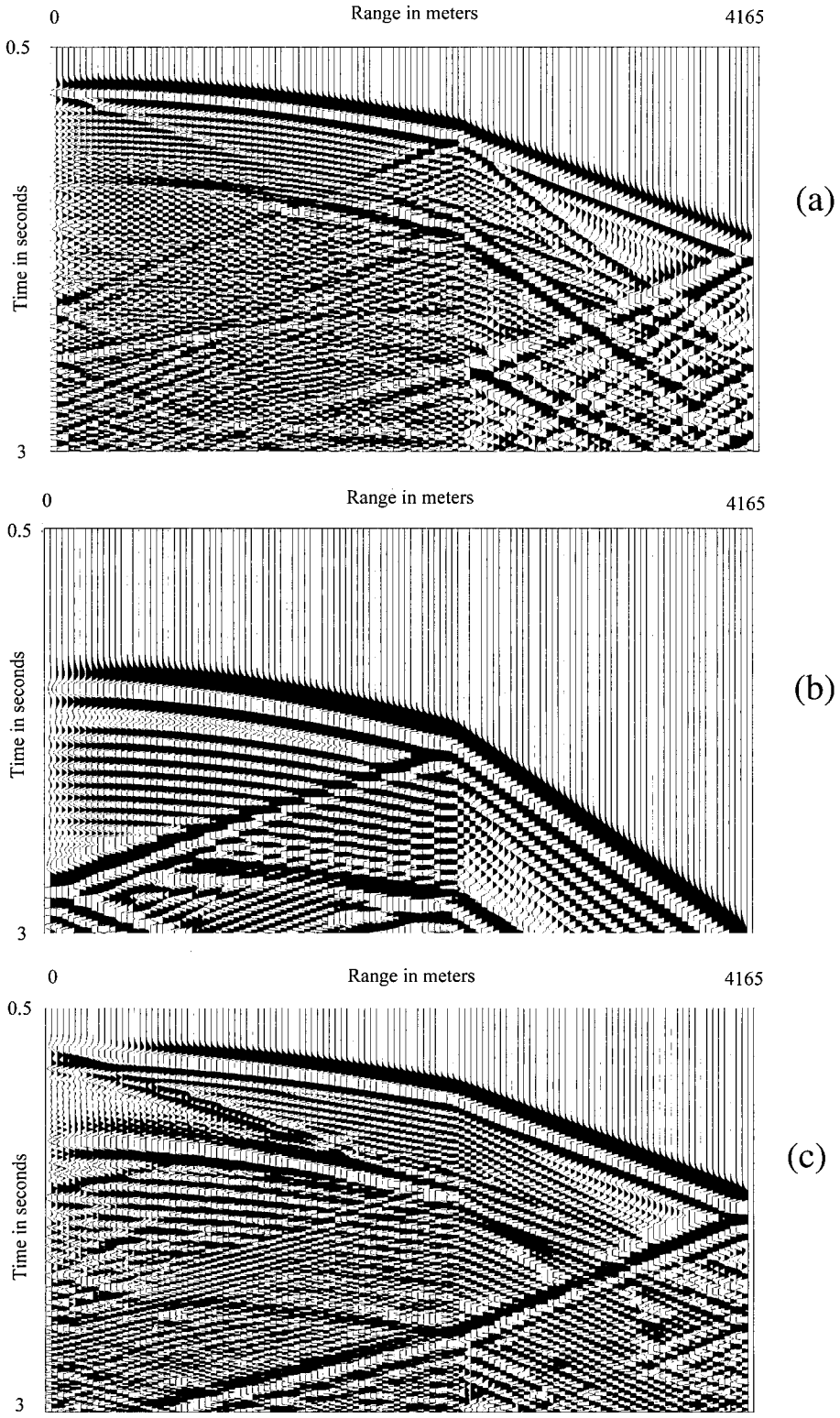

Figure 2. Three-component synthetic seismograms for Model 2, generated by the finite-difference method without absorbing boundary conditions. (a) u_x component (b) u_y component (c) u_z component.

and requires a small amount of storage space as only three nearest grid points are involved in a direction. Our method has two important stages: diffusion and compensation steps besides the conventional finite-difference computations. Although the FCT-based FD method adds the diffusion (Stage 2) and offsetting (Stage 3) calculations resulting in added computation costs in comparison with the conventional FD method, it offers the opportunity to use a coarse grid to obtain the same accuracy that is comparable to the conventional FD method on a fine grid. Therefore, the total computational costs of the FCT

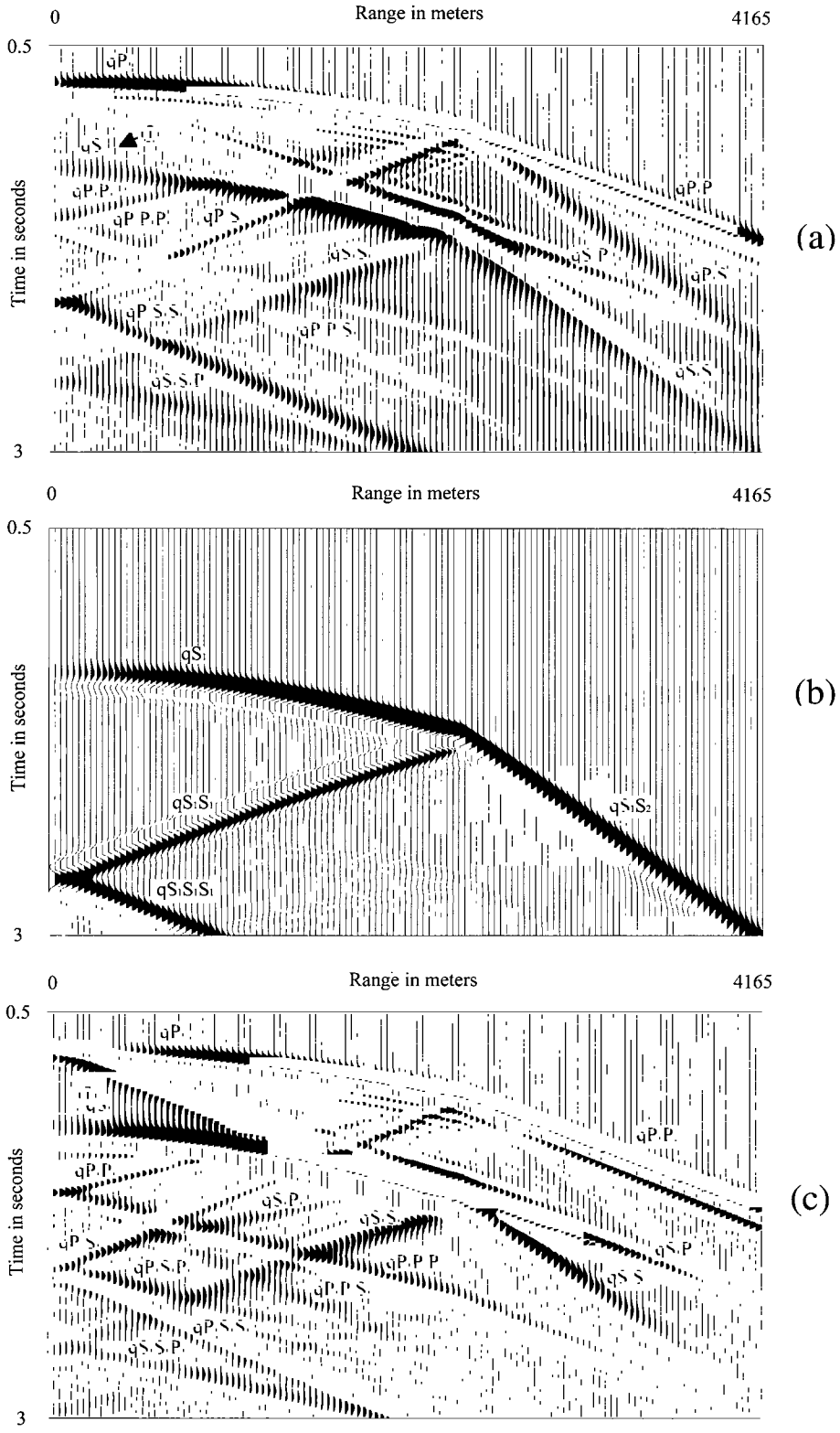

Figure 3. Three-component synthetic seismograms for Model 2, generated by the FCT based FD with a 2–times absorbing boundary condition. Where ① denotes the *P*- to *S*- converted wave. (a) u_x component (b) u_y component (c) u_z component.

based FD do not exceed that of the conventional FD methods on a fine grid, and are more efficient than standard FD. In addition, the diffusion and offsetting stages are independent of the finite-difference stage, so it is easy to implement the parallel calculations for the diffusion and offsetting and this will further increase the computational efficiency of the FCT based FD.

Provided a suitable time increment, not only stable calculations can be kept, but also iterative speed can be improved

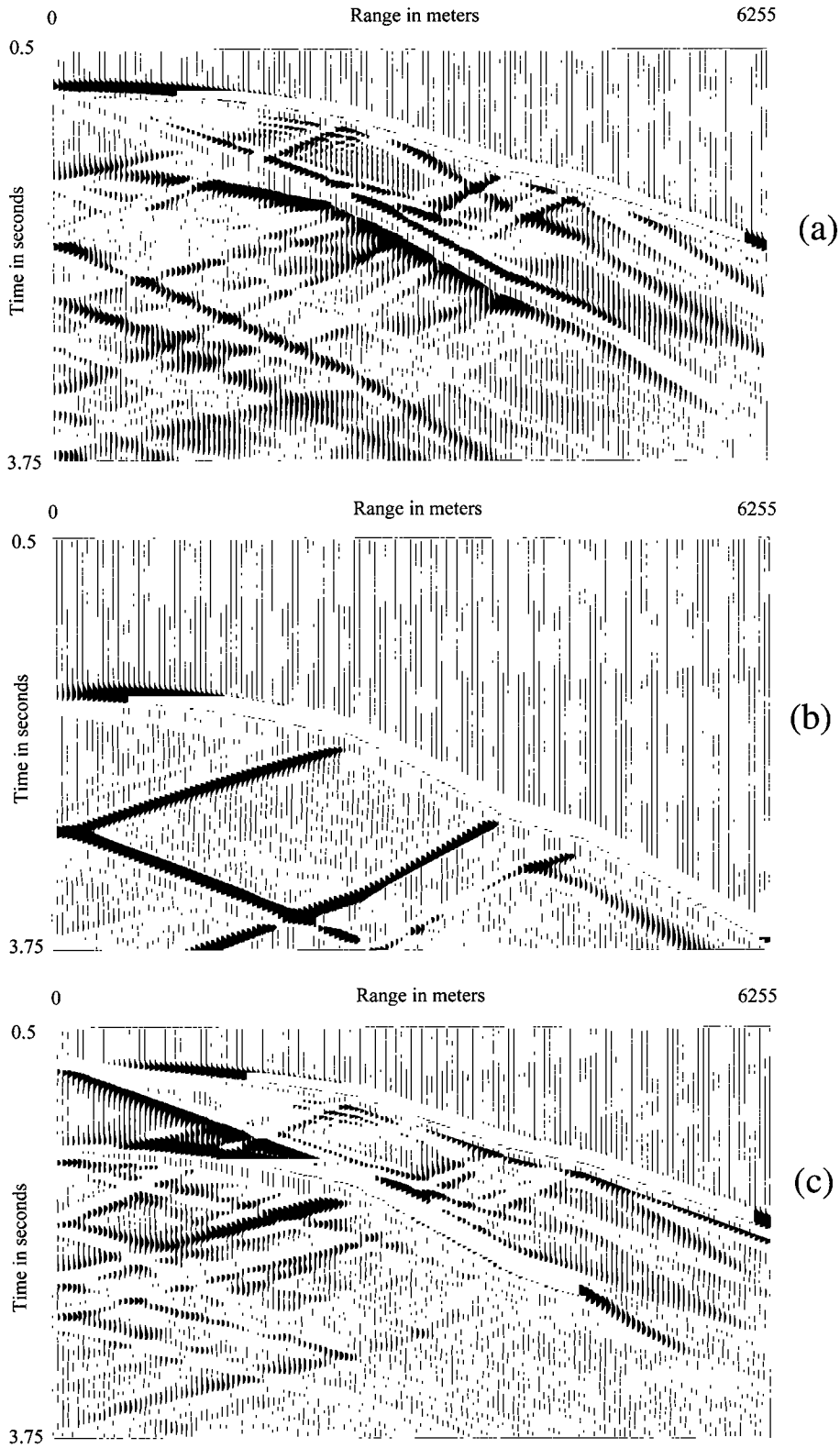

Figure 4. Three-component synthetic seismograms for Model 3, generated by the FCT based FD with the 2–times absorbing boundary conditions. (a) u_x component (b) u_y component (c) u_z component.

while the spatial increment is a constant. We have obtained the stability criterion based on the modulus of the elastic stiffness matrices. A new absorbing boundary condition has been given to the elastic wave equations in anisotropic media. The absorbing boundary conditions have n-times absorbing ability and are decoupled for three-displacement components. The property is very useful to reduce the errors introduced in discretizing the absorbing boundary equations. Moreover, we have given a

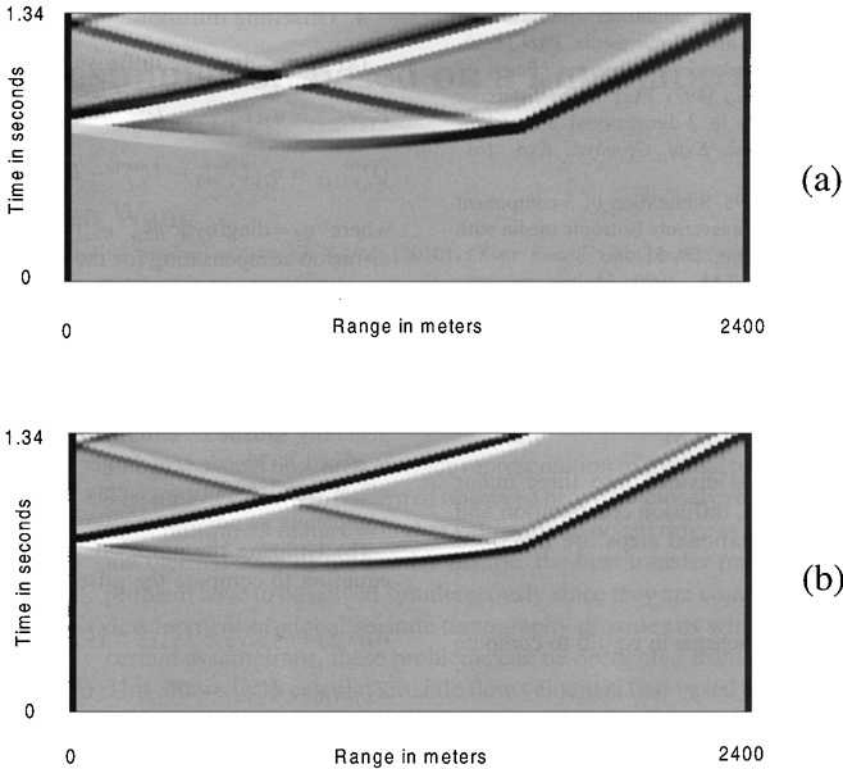

Figure 5. Comparison of FCT and FD methods: (a) acoustic synthetic seismograms generated by the FCT with a grid step size $\Delta x = \Delta z = 24$ m; (b) acoustic synthetic seismograms generated by the 4th-order staggered grid FD with a grid step size $\Delta x = \Delta z = 8$ m.

stable discrete formula for the absorbing condition while the absorbing times $n = 2$. Synthetic seismograms in Figs 3 and 4 show that the n–times decoupled absorbing boundary conditions are very effective.

As we have seen, the FCT technique can effectively suppress the numerical dispersion that arise in the FD algorithms when a too coarse grid is used or large gradients and even discontinuities in the wavefield are involved. In data processing noise due to source location at grid points caused are usually inevitable. Actually, these noise presented in numerical modelling is a spurious oscillation or unphysical ripples. In wavefield simulations, the source-noise is also an important factor of lowering the resolution of the numerical synthetic seismograms. Fortunately, from Fig. 3 as compared with Fig. 2 we can clearly see that the FCT technique can eliminate successfully the noises caused by seismic sources located at grid points in the finite difference implementation.

ACKNOWLEDGMENTS

We thank Dr Wang Guangjie for providing the image software. The work was financially supported through the National Natural Science Foundation of China (No. 40174012). We thank Professor H. Schmeling (Editor), Dr T. Bergmann (the reviewer) and an anonymous reviewer for their constructive comments that greatly improve the readability of this paper.

REFERENCES

Aboudi, J., 1971. The motion excited by an impulsive source in an elastic half-space with a surface obstacle, *Bull. seism. Soc. Am.*, **61,** 747–763.

Book, D.L., Boris, J.P. & Hain, K., 1975. Flux-corrected transport II: generalization of the method, *J. Comput. Phys.*, **18,** 248–283.

Booth, D.C. & Crampin, S., 1983a. The anisotropic reflectivity technique: theory, *Geophys. J. R. astr. Soc.*, **72,** 755–765.

Booth, D.C. & Crampin, S., 1983b. The anisotropic reflectivity technique: anomalous arrives from an anisotropic upper mantle, *Geophys. J. R. astr. Soc.*, **72,** 767–782.

Boris, J.P. & Book, D.L., 1973. Flux-corrected transport, I. SHASTA, A fluid transport algorithm that works, *J. Comput. Phys.*, **11,** 38–69.

Chang, W.F. & McMechan, G.A., 1989. Absorbing boundary conditions for 3-D acoustic and elastic finite-difference calculations, *Bull. seism. Soc. Am.*, **79,** 211–218.

Clayton, J.F. & Engquist, B., 1977. Absorbing boundary conditions for acoustic and elastic wave equations, *Bull. seism. Soc. Am.*, **67,** 1529–1540.

Faria, E.L. & Stoffa, P.L., 1994. Finite-difference modelling in transversely isotropic media, *Geophysics,* **59,** 282–289.

Fei, T. & Larner, K., 1995. Elimination of numerical dispersion in finite-difference modelling and migration by flux-corrected transport, *Geophysics,* **60,** 1830–1842.

Higdon, R.L., 1987. Numerical absorbing boundary conditions for the wave equation, *Math. Comp.*, **49,** 65–90.

Igel, H., Mora, P. & Riollet, B., 1995. Anisotropic wave propagation through finite-difference grids, *Geophysics,* **60,** 1203–1216.

Randal, C.J., 1988. Absorbing boundary condition for the elastic wave equation, *Geophysics,* **53,** 611–624.

Richtmyer, R.D. & Morton, K.W., 1967. *Difference Methods for Initial Value Problems,* Interscience, New York.

Sockacki, J., Kubichek, R., George, J., Fletcher, W.R. & Smithson, S., 1987. Absorbing boundary conditions and surface waves, *Geophysics,* **52,** 60–71.

Tsingas, C., Vafidis, A. & Kanasewich, E.R., 1990. Elastic wave propagation in transversely isotropic media using finite-differences, *Geophys. Prospect.*, **38,** 933–949.

Yang, D.H., 1996. A study of forward simulation and inversion methods of seismic wave equations in anisotropic media, *PhD Thesis,* Institute of Geophysics, Chinese Academy of Sciences, China.

Yang, D.H., Mu, Y.G. & Di, B.R., 1997. FCT finite-difference modelling for VSP seismic records in 2-dimensional anisotropic media, *67th Ann. Internat. Mtg, Soc. Expl. Geophys., Exp. Abs.,* 1513–1516.

Zhang, Z.J., He, Q.D. & Teng, J., 1993. Simulation of 3-component seismic records in a 2-dimensional transversely isotropic media with finite-difference, *Can. J. Expl. Geophys.,* **29,** 51–58.

Zhang, Z.J., Wang, G.J. & Harris, J.M., 1999. Multi-component wavefield simulation in viscous extensively dilatancy anisotropic media, *Phys. Earth planet Inter.,* **114,** 25–38.

APPENDIX: THE FCT FINITE-DIFFERENCE ALGORITHM

In general, the FCT based FD is divided into three major steps (finite-difference calculations, diffusion computation and offsetting diffusion). The computational steps are described below.

1. Providing initial value $U_{i,j}^0$;
2. Utilizing the finite-difference scheme in eq. (2) to compute $U_{i,j}^{n+1}$, where $n \geq 0$;
3. Diffusion computation

(a) Computing diffusive fluxes at the nth time-step:

$$P_{i+1/2,j}^n = \eta_1 (U_{i+1,j}^n - U_{i,j}^n - U_{i+1,j}^{n-1} + U_{i,j}^{n-1}),$$

$$Q_{i,j+1/2}^n = \eta_1 (U_{i,j+1}^n - U_{i,j}^n - U_{i,j+1}^{n-1} + U_{i,j}^{n-1}),$$

where $\eta_1 = \mathrm{diag}(\eta_{1x}, \eta_{1y}, \eta_{1z})$ is a diagonal matrix. The elements η_{1x}, η_{1y} and η_{1z} are the smooth parameters for three displacement components u_x, u_y and u_z, respectively. Usually, $0 \leq \eta_{1j} \leq 1$ $(j=1, 2, 3)$, and they can be chosen as some constants. The larger the value of η_{1j}, the more complete is the elimination of numerical dispersion and source-noises, also the more serious is the amplitude loss of true ripples. The value is often determined from a few small-scale numerical experiments. We find that $0.008 \leq \eta_{1j} \leq 0.05$ $(j=1, 2, 3)$ is acceptable in our numerical examples. Of course, η_{1j} can also be a function (e.g. linear).

(b) Through diffusive fluxes P and Q, we smooth the numerical solutions of the eq. (2) to eliminate grid dispersion and source noises.

$$\bar{U}_{i,j}^{n+1} = U_{i,j}^{n+1} + (P_{i+1/2,j}^n - P_{i-1/2,j}^n) + (Q_{i,j+1/2}^n - Q_{i,j-1/2}^n).$$

4. Offsetting diffusion

(a) Computing the diffusive fluxes at time-step $n+1$:

$$\bar{P}_{i+1/2,j}^{n+1} = \eta_2 (U_{i+1,j}^{n+1} - U_{i,j}^{n+1} - U_{i+1,j}^n + U_{i,j}^n),$$

$$\bar{Q}_{i,j+1/2}^{n+1} = \eta_2 (U_{i,j+1}^{n+1} - U_{i,j}^{n+1} - U_{i,j+1}^n + U_{i,j}^n),$$

where $\eta_2 = \mathrm{diag}(\eta_{2x}, \eta_{2y}, \eta_{2z})$ is a diagonal matrix of the diffusion compensating for the amplitude losses of true ripples in removing the numerical dispersion. The elements η_{2x}, η_{2y} and η_{2z} are the compensation parameters for three displacement components (u_x, u_y and u_z) or for three amplitude components in x-, y-, and z-directions, respectively. These parameters can be chosen as some constants and $0 \leq \eta_{2j} \leq 1$ $(j=1, 2, 3)$ is generally satisfied. Actually, the value of η_{2j} $(j=1, 2, 3)$ that is about 8–20 per cent larger than η_{2j} $(j=1, 2, 3)$ is used in offsetting calculations so as to recover the true ripples as completely as possible.

(b) Utilizing the modified and the solution of difference equation to compute the offsetting diffusive fluxes:

$$X_{i+1/2,j} = \bar{U}_{i+1,j}^{n+1} - U_{i+1,j}^n - (\bar{U}_{i,j}^{n+1} - U_{i,j}^n)$$

$$Z_{i,j+1/2} = \bar{U}_{i,j+1}^{n+1} - U_{i,j+1}^n - (\bar{U}_{i,j}^{n+1} - U_{i,j}^n)$$

(c) Ultilizing the offsetting diffusive fluxes and modifying the modified solution $\bar{U}_{i,j}^{n+1}$, again, then we obtain corrected solution

$$U_{i,j}^{n+1} = \bar{U}_{i,j}^{n+1} - (\bar{X}_{i+1/2,j} - \bar{X}_{i-1/2,j}) - (\bar{Z}_{i,j+1/2} - \bar{Z}_{i,j-1/2}),$$

where,

$$\bar{X}_{i+1/2,J} = (s_m^x \cdot \max\{0, \min[s_m^x \cdot x_{m,i-1/2,j}, \bar{U}_{i+1,j}^{n+1} - \bar{U}_{i,j}^{n+1}), s_m^x \cdot x_{m,i+3/2,j}]\})_{3\times 1},$$

$$\bar{Z}_{i,j+1/2} = (s_m^z \cdot \max\{0, \min[s_m^z \cdot z_{m,i,j-1/2}, \bar{U}_{i,j+1}^{n+1} - \bar{U}_{i,j}^{n+1}), s_m^z \cdot z_{m,i,j+3/2}]\})_{3\times 1},$$

$$S^x = (s_m^x)_{3\times 1} = (sign(\bar{p}_{m,i+1/2,j}^{n+1}))_{3\times 1},$$

$$S^z = (s_m^z)_{3\times 1} = (sign(\bar{q}_{m,i,j+1/2}^{n+1}))_{3\times 1},$$

where $m=1, 2, 3$, and the footnote m denotes the mth element in these vectors $\boldsymbol{X}$, $\boldsymbol{Z}$, $\boldsymbol{S}^x$ and $\boldsymbol{S}^z$.